J Neurophysiol 108: 3233–3238, 2012.
First published September 19, 2012; doi:10.1152/jn.01058.2011.

Upper threshold of extracellular neural stimulation

David Boinagrov,[1,2] Susanne Pangratz-Fuehrer,[1,3] Bongsoo Suh,[4] Keith Mathieson,[1] Natasha Naik,[1,3] and Daniel Palanker[1,3]

[1]*Hansen Experimental Physics Laboratory, Stanford University, Stanford, California;* [2]*Department of Physics, Stanford University, Stanford, California;* [3]*Department of Ophthalmology, School of Medicine, Stanford University, Stanford, California; and* [4]*Department of Electrical Engineering, Stanford University, Stanford, California*

Submitted 21 November 2011; accepted in final form 18 September 2012

Boinagrov D, Pangratz-Fuehrer S, Suh B, Mathieson K, Naik N, Palanker D. Upper threshold of extracellular neural stimulation. *J Neurophysiol* 108: 3233–3238, 2012. First published September 19, 2012; doi:10.1152/jn.01058.2011.—It is well known that spiking neurons can produce action potentials in response to extracellular stimulation above certain threshold. It is widely assumed that there is no upper limit to somatic stimulation, except for cellular or electrode damage. Here we demonstrate that there is an upper stimulation threshold, above which no action potential can be elicited, and it is below the threshold of cellular damage. Existence of this upper stimulation threshold was confirmed in retinal ganglion cells (RGCs) at pulse durations ranging from 5 to 500 μs. The ratio of the upper to lower stimulation thresholds varied typically from 1.7 to 7.6, depending on pulse duration. Computational modeling of extracellular RGC stimulation explained the upper limit by sodium current reversal on the depolarized side of the cell membrane. This was further confirmed by experiments in the medium with a low concentration of sodium. The limited width of the stimulation window may have important implications in design of the electro-neural interfaces, including neural prosthetics.

neural; prosthesis; retinal; stimulation

EXTRACELLULAR NEURAL STIMULATION is used in retinal (Palanker et al. 2005; Rizzo and Wyatt 1997; Weiland et al. 2005; Zrenner et al. 2011) and cochlear prostheses (House and Urban 1973; Spelman 1999; Zierhofer et al. 1995), in deep brain stimulation (Kern and Kumar 2005; Kringelbach et al. 2007; Mayberg et al. 2005; Perlmutter and Mink 2006) as treatment for Parkinson's disease (Breit et al. 2004; Plaha and Gill 2005), dystonia (Krauss et al. 2004; Vercueil et al. 2001), and chronic headaches (Kumar al. 1997 Leone 2006), and in several other applications of electro-neural interfaces (Godec et al. 1975; Kimberley et al. 2004; Long et al. 1981). In all of these applications, the characteristics of the stimulation waveform (principally the amplitude, polarity, and pulse width) play an important role in the design of a particular prosthetic device, making it critical to understand the relationship between stimulation threshold and pulse duration. Electrical stimulation of the retinal ganglion cells (RGC), used in epiretinal prostheses, was extensively studied by several research groups (Fried et al. 2006; Jensen et al. 2003, 2005; Sekirnjak et al. 2006, 2008; Stett et al. 2000, 2007; Tsai et al. 2009), and the strength-duration relationship has been experimentally measured (Jensen et al. 2003, 2005; Sekirnjak et al. 2006; Tsai et al. 2009) and modeled computationally (Boinagrov et al. 2010; Greenberg et al. 1999). The strength-duration relationship defines for a given pulse duration the minimum stimulus strength, or stimulation threshold, above which an action potential (AP) is generated. It is generally assumed that a neuron will elicit AP at any stimulus strength above the threshold, and the upper limit is defined only by the cellular damage (Butterwick et al. 2007; McCreery et al. 1990) or by the limits of irreversible electrochemistry on stimulating electrode (Brummer and Turner 1977; Cogan et al. 2004).

Recent computational studies (Boinagrov et al. 2010), based on the ion channel model for RGCs, predicted the existence of a stimulation upper threshold, above which no spiking could be elicited. Experimental evidence of this phenomenon in RGCs has not been reported. An experimental study of the cultured dorsal root ganglia (Buitenweg et al. 2002) described an observation of the upper threshold of stimulation, but only in very specific conditions of a neuron in culture sealing the stimulation microelectrode. An open question remained, however, as to how general or widespread this phenomenon is and if it can be observed in extracellular stimulation of a real neural tissue.

It is a common practice, in electro-neural interfaces in general and in prosthetic devices in particular, to deliver currents well above the threshold to ensure effective stimulation. Existence of the upper stimulation threshold places a limit on the current that should be delivered to a target neuron. The window between the upper and lower thresholds may be quite narrow, making it very important to carefully optimize the stimulus strength and duration to provide reliable neural responses. The present study describes the dependence of the upper stimulation threshold in RGCs on pulse duration. It also explains the biophysical mechanism of this phenomenon, using computational model of neural stimulation, with further confirmation by the experiments in low-sodium extracellular solution.

MATERIALS AND METHODS

Retinal preparation. Wild-type Long-Evans rat (Charles River Laboratories International, Wilmington, MA) retinas were used for these experiments. Postnatal *day 45–80* animals were anesthetized by inhalation of evaporated isoflurane (1 g/l; Baxter Healthcare, Deerfield, IL) and subsequently euthanized with Beuthanasia-D (1 ml/kg animal weight; Schering-Plough Animal Health, Union, NJ) in accordance with the protocol approved by the Stanford University Administrative Panel on Laboratory Animal Care. The eyes were enucleated and dissected in the Ames' medium (Sigma-Aldrich, St. Louis, MO) bubbled with a mixture of 95% O_2 and 5% CO_2 (Airgas, Redwood City, CA). After the sclera was dissected, the retina was detached from the pigment epithelium. If the vitreous humor was attached to the retina, it was removed with the use of cotton tips or with the addition of hyaluronic acid (0.025 mg/ml; Sigma-Aldrich) in the Ames' me-

Address for reprint requests and other correspondence: D. Boinagrov, 452 Lomita Mall, Stanford, CA 94305 (e-mail: boinagrov@gmail.com).

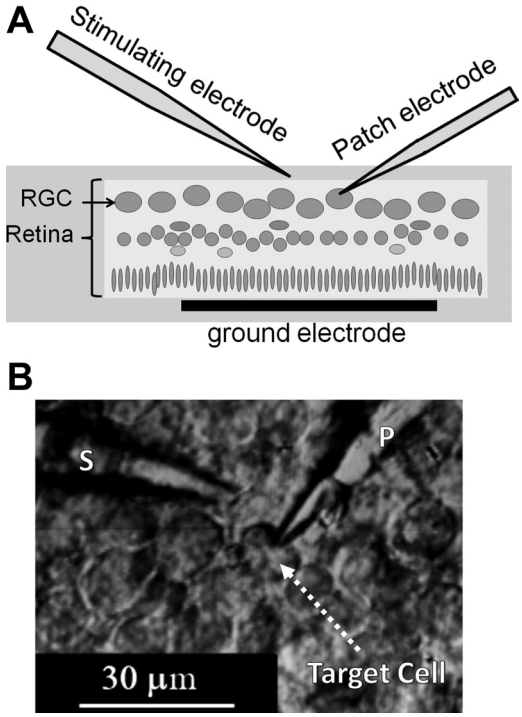

Fig. 1. In vitro patch-clamp recording from retinal ganglion cells (RGCs) in the isolated retina during extracellular stimulation. *A*: schematic diagram of stimulation and recording. *B*: differential interference contrast microscope image of the RGC layer. A 1- to 2-μm patch pipette (P) is attached to the target cell; the 4-μm stimulation pipette (S) is held near the cell.

dium for 7 min. The retina was then cut into pieces ~1 mm^2 in size, attached to filter paper, and placed in the perfusion chamber photoreceptor side down (see Fig. 1*A*), where it was perfused by 5 ml/min of artificial cerebrospinal fluid (ACSF; containing in mM: 126 NaCl, 10 glucose, 2.5 KCl, 1.25 $NaH_2PO_4{\cdot}H_2O$, 1 $MgSO_4{\cdot}7H_2O$, 2 $CaCl_2{\cdot}2H_2O$, and 26 $NaHCO_3$) bubbled with 95% O_2 and 5% CO_2. The low-sodium solution (containing in mM: 110 choline chloride, 10 glucose, 2.5 KCl, 1.25 $NaH_2PO_4{\cdot}H_2O$, 10 $MgSO_4{\cdot}7H_2O$, 0.5 $CaCl_2{\cdot}2H_2O$, and 26 $NaHCO_3$) was used for perfusion instead of ACSF where specified.

Stimulation and recording. The patch-clamp technique (Sakmann and Neher 1984) was used to record the cell potential of individual RGCs (see Fig. 1*B*). Micropipettes were pulled from borosilicate glass tubes with a Sutter P-2000 pipette puller (Sutter Instrument, Novato, CA). Patch pipettes were filled with a solution containing (in mM) 117 KCl, 4 Mg-ATP, 0.3 Na_2-GTP, 20 Na_2-creatine phosphate, 10 HEPES, and 0.2 EGTA (all from Sigma-Aldrich) with pH of 7.3. A silver-chloride electrode was immersed in the patch pipette, and a large silver wire placed in the petri dish was used as a reference electrode. Successful patching was performed with micropipettes with resistance of 5–15 MΩ. Signal recording was performed at 33–35°C temperature with a Multiclamp 700A amplifier (Molecular Devices, Sunnyvale, CA), digitized with a Digidata 1440 data acquisition system (Molecular Devices), and recorded on a personal computer with pClamp 10.2 software (Molecular Devices).

Stimulation pulses were delivered by another micropipette filled with ACSF and with a thick silver or platinum wire electrode immersed into it. The pipette tip of 3–30 μm in diameter was placed 25 $\pm$ 15 μm from the target cell. Rectangular monophasic cathodic pulses were generated with an isolated pulse stimulator (model 2100; A-M Systems, Carlsborg, WA) and delivered at a repetition rate of 1 Hz. The pulse duration was varied from 1 μs to 5 ms, and stimulating current from 0.5 μA to 5 mA. The rectangular shape of the stimulation current was verified by measuring the voltage drop on a resistor connected in series with the stimulation pipette. For each stimulus duration and strength, at least 10 stimulation sweeps of 1 s in duration were recorded.

Numerical modeling. A previously described (Boinagrov et al. 2010) computational model of extracellular stimulation in RGCs, based on five-ion channel approximation (Fohlmeister and Miller 1997), was used with the minor modifications explained below.

RESULTS

Data from 26 cells were recorded in 16 retinal preparations. Monophasic cathodic current pulses were delivered through the extracellular stimulation electrode positioned close to the target cell. For the fixed stimulus duration, the current (I) was increased until the stimulation threshold was reached, when the short-latency (<4 ms) APs were generated (see Fig. 2, I = 3 μA and 5 μA). The current was further increased until the stimulation upper threshold was reached, where the AP was not elicited anymore (see Fig. 2, I = 18 μA and 22 μA). The current was then decreased below the upper stimulation threshold to verify the cell viability and elicitation of the APs. A characteristic spontaneous AP recorded in the same measurement is depicted in Fig. 2 for comparison. This procedure was repeated for multiple pulse durations.

Figure 3*A* shows the variation of the AP elicitation probability with stimulus magnitude for pulses of 0.1 ms in duration. Elicitation probability is 0% below the lower threshold and increases to 100% above it. It then remains at 100% until the stimulus magnitude approaches the upper threshold, and drops down to 0% above this upper threshold. By interpolating the stimulation threshold between the measured data points (solid lines in Fig. 3*A*), we find the stimulation thresholds, at which the elicitation probability reaches 50%. The lower of these two

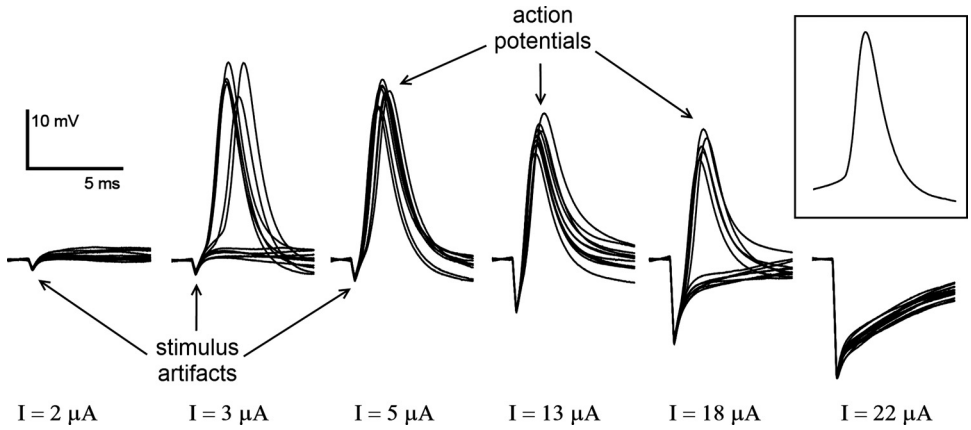

Fig. 2. A series of cellular traces with increasing stimulus strength and fixed duration of 0.2 ms. Action potentials (APs) were elicited for stimulus current (I) from 5 to 13 μA and in about one-half of all sweeps for I = 3 and 18 μA; APs could not be elicited below I = 2 μA and above I = 22 μA. *Inset* at *right* illustrates a spontaneous AP, for comparison.

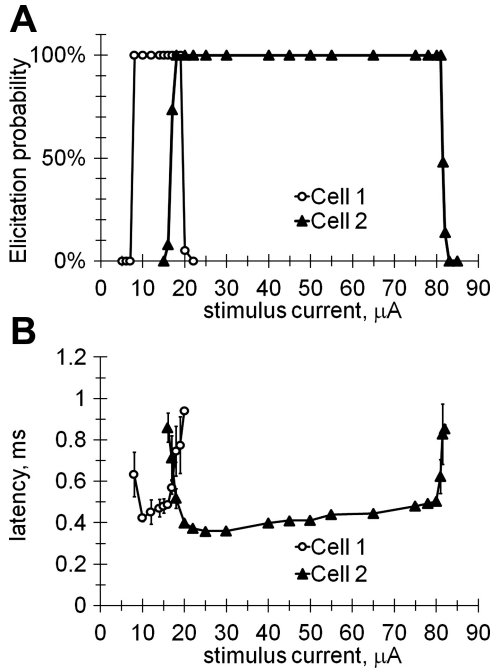

Fig. 3. Spiking elicited by 0.1-ms cathodic pulses as a function of the stimulus current shown for 2 different RGCs located at different distances from the stimulating electrode. *A*: probability of eliciting the APs. *B*: latency of elicited AP. Error bars correspond to the standard deviation of successive recordings. The number of independent data points shown for *cell 1* is 14 and for *cell 2* is 21.

we call the stimulation lower threshold (I_{LT}), with the higher one being the stimulation upper threshold (I_{UT}). In the cases shown in Fig. 3, these values are $I_{LT} = 7.5$ μA, $I_{UT} = 19.5$ μA for *cell 1* and $I_{LT} = 17$ μA, $I_{UT} = 81$ μA for *cell 2*. When the stimulus amplitude was increased above the upper threshold and subsequently decreased, the stimulation thresholds did not vary by more than 10% from the levels obtained on the rising phase of the measurement. This lack of significant hysteresis indicates independence of the thresholds on stimulation history.

Figure 3*B* shows the corresponding AP latency, which is defined as the time interval between the stimulus onset and the maximum voltage of the AP. The latency plot has a characteristic U-shape, with lower values in the middle of the stimulation window and a rapid increase near the upper and lower thresholds. Near the threshold values the latency variation also increased, as illustrated by the error bars.

The lower and upper stimulation thresholds were measured for different stimulus durations to obtain the strength-duration dependence shown in Fig. 4 for a single typical cell. The circles indicate the current and duration for the points where the AP elicitation probability is above 50%, and the crosses indicate where it is below 50%. For most of these points, the elicitation probability is 100% for the disks or 0% for the crosses, except for the points close to the lower and upper thresholds, where some intermediate values have been observed. The lower and upper thresholds were fitted with the power curves with the rheobase. The stimulation upper threshold was observed for six different stimulus durations at or below 0.5 ms.

The upper threshold of stimulation was clearly observed with at least one pulse duration in 21 of the 26 recorded cells (from 12 preparations). In the remaining 5 neurons, the stimulus artifact strongly interfered with the elicited AP, making the determination of the upper threshold unreliable.

Stimulation thresholds varied significantly from cell to cell. For example, with 0.5-ms pulses, the stimulation lower threshold varied from 0.4 to 4.4 μA, and with 0.2-ms pulses, from 2.3 to 12 μA. This variability is likely due to the differences in cell sizes, shapes, and position relative to the stimulation electrode.

The dynamic range of stimulation, or the stimulation window, can be defined as the ratio of the upper and lower thresholds for any pulse duration. For the cell shown in Fig. 4, the stimulation window varied with pulse duration from 1.7 $\pm$ 0.5 to 5.0 $\pm$ 1.7. The stimulation window also varied from one cell to another. For example, for 0.2-ms pulses, the upper threshold was observed in 15 cells and the stimulation window varied from 2.0 $\pm$ 0.2 to 7.6 $\pm$ 1.1 (with an average of 3.7), whereas for 0.5-ms pulses, in 14 cells the stimulation window varied mostly from 1.8 $\pm$ 0.4 to 6.4 $\pm$ 1.9, even reaching 16.3 $\pm$ 5.3 in a single cell (with an average of 4.6).

Retinal stimulation in low-sodium medium. To verify the hypothesis that stimulation upper threshold is caused by the sodium current reversal, the ACSF perfusion medium with the sodium concentration of $[Na]_0 = 153$ mM was replaced with a low-sodium solution having a concentration of $[Na]_1 = 27.3$ mM. RGC stimulation upper threshold was initially determined with the use of the ACSF perfusion medium, and then again with the low-sodium solution, while keeping the patch pipette attached to the same cell. For the 5 cells recorded, the stimulation upper threshold at 0.5 ms decreased in low-sodium medium by a factor of 1.67 $\pm$ 0.33, compared with the normal medium, whereas the resting potential did not change.

DISCUSSION

Computational modeling of extracellular stimulation. A computational model of extracellular stimulation in RGCs, based on a five (plus leakage)-ion channel model (Fohlmeister and Miller 1997), was recently described (Boinagrov et al. 2010). One of the features predicted by that model was the existence of the upper stimulation threshold, caused by the reversal of sodium ion current. The other feature was the U-shaped dependence of the latency of the elicited AP on stimulus strength. As shown in Fig. 3*B*, the experimental latency plot has indeed a characteristic U-shape, with lower values in the middle of the stim-

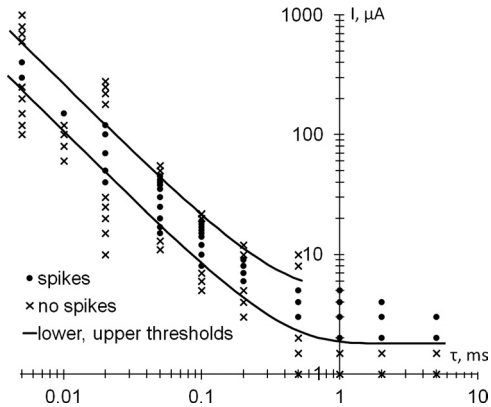

Fig. 4. Strength-duration dependence of the upper and lower thresholds of stimulation for rectangular cathodic pulses. The stimulation range (spikes, ●) lies between the lower and upper stimulation thresholds. No APs are elicited outside this range (no spikes, ×). The lower and upper thresholds are defined as having a 50% elicitation probability. The number of independent data points shown is 86; τ, stimulus duration.

ulation window and rapid increase near the upper and lower thresholds.

The dotted line in Fig. 5*A* depicts the modeled strength-duration relationship, as taken from Boinagrov et al. (2010). In this example the lower and upper thresholds intersect at a pulse duration of about 55 μs, below which no stimulation is possible. This behavior differs from the experimental measurements shown in Fig. 4, where the upper and lower threshold curves do not intersect, at least for durations above 5 μs. To explore this mismatch, we performed additional computational simulations using the same basic model configuration and ion channel composition (Fohlmeister and Miller 1997). When the maximum sodium channel conductivity ($\bar{g}_{Na}$) in the model increased from 50 to 85 mS/cm^2 (corresponding to the higher concentration of sodium ion channels on cell membrane), the strength-duration relationship of the upper and lower thresholds, depicted by the dashed curve in Fig. 5*A*, corresponded qualitatively much better to the experimental data shown in Fig. 4. Variation of the conductivity of potassium channels in the computational model did not significantly affect the shape of the strength-duration curve.

We also explored an asymmetric distribution of sodium ion channels in the cell, which models the effect of the increased ion channel density at the axonal hillock. Here it can be 2–40 times higher than the average on the soma (Fried et al. 2009). For this asymmetric configuration, the sodium channel maximum conductivity was increased 10-fold (to 500 mS/cm^2) at the depolarized pole of the cell, accounting for 5% of the total area, as shown in Fig. 5*B*. This yielded a strength-duration curve (thin solid lines in Fig. 5*A* for the case of cathodic pulses delivered via epiretinal electrode) with upper and lower thresholds similar to the case of a uniform distribution of sodium channels at high density (dashed curves).

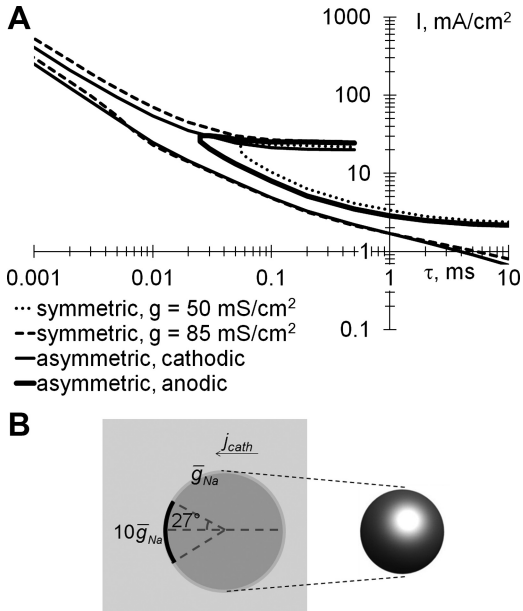

Fig. 5. *A*: modeled strength-duration dependences of the upper and lower thresholds of stimulation for rectangular monophasic pulses. Curves are shown for symmetric soma with a sodium ion channel conductivity ($\bar{g}_{Na}$) of 50 mS/cm^2 (dotted line)or 85 mS/cm^2 (dashed line) and asymmetric soma stimulated with cathodic (solid thin line) and anodic pulses (solid thick line) applied via epiretinal electrode. *B*: model of an asymmetric soma stimulated with a cathodic pulse (j_{cath}).

The asymmetry introduced by the presence of the modeled axonal hillock resulted in a very different appearance of the stimulation thresholds for cathodic (thin solid line in Fig. 5*A*) and anodic pulses (thick solid line). Since axonal hillocks are in the upper part of RGCs facing the epiretinal electrode and anodic pulses depolarize the opposite side of RGC, the area with low sodium channel concentration, the strength-duration curve looks qualitatively similar to the one for symmetric soma and low sodium conductivity (dotted line). Cathodic pulses from epiretinal electrode depolarize the area of axonal hillock (higher conductivity), resulting in reduced stimulation threshold. This difference between the lower stimulation thresholds for cathodic and anodic pulses has been observed experimentally in epiretinal stimulation (Jensen et al. 2005; Sekirnjak et al. 2006). For subretinal stimulation of the same type of asymmetric cells, the cathodic and anodic curves would be swapped. Therefore, the stimulation thresholds with anodic pulses in subretinal configuration should be lower than with cathodic pulses, as was indeed observed experimentally (Jensen and Rizzo 2006).

Mechanism of the upper threshold. According to the computational model (Boinagrov et al. 2010), the upper threshold of stimulation is caused by reversal of the sodium ion channel current at strong depolarizations. For the sodium inflow, the current density is defined (Hodgkin and Huxley 1952) as $j_{Na} = g_{Na}\cdot(E_{Na} - V)$, where g_{Na} is sodium channel conductivity, E_{Na} is the sodium reversal potential (typically in the range of 35–50 mV), and V is the local transmembrane voltage. During the stimulus, the sodium ion channels are activated at the depolarized part of the cell membrane, increasing g_{Na} and j_{Na} and thus letting the positive sodium current into the cell, which may trigger the AP. At high stimuli, when V approaches E_{Na}, the term ($E_{Na} - V$) approaches zero and reduces the sodium inflow, j_{Na}. When the total sodium inflow in the cell is insufficient for generating the AP, the stimulation upper threshold is observed. At higher stimuli, when V exceeds E_{Na}, j_{Na} becomes negative. Sodium ions flow out of the cell through open ion channels, and no AP is generated.

To verify the hypothesis that stimulation upper threshold is caused by the sodium current reversal, additional measurements were performed in a low-sodium medium. Reduction of the extracellular sodium concentration from $[Na]_0 = 153$ mM to $[Na]_1 = 27.3$ mM decreases the sodium channel reversal potential by

$$\Delta V = \frac{kT}{e}\cdot \ln\frac{[Na]_0}{[Na]_1} = 45 \text{ mV}.$$

According to the model (Boinagrov et al. 2010), this should reduce the stimulation upper threshold by a factor of 1.56 for pulses 0.5 ms in duration, compared with the normal values of E_{Na}. Experimental observations of the decreasing upper threshold by a factor of 1.67 ± 0.33 confirm model prediction, further supporting the hypothesis that the sodium current reversal is the mechanism behind the stimulation upper threshold. Calcium ion channels have much higher reversal potential of 110–160 mV (Fohlmeister and Miller 1997), and therefore the calcium current reversal will occur at stimuli exceeding those of sodium current reversal.

It is important to distinguish the upper threshold of somatic stimulation observed in the current study from the effect of

anodal surround block of the AP propagation in the axon (Jankowska and Roberts 1972; Katz and Miledi 1965; Ranck 1975). The latter phenomenon describes hyperpolarization of the axon, which stops the propagation of the AP generated in other parts of that cell. In contrast, the current study is based on the direct measurements of the AP in the cell soma, measured with a patch clamp. It demonstrates inability of strong stimuli to produce AP in the soma, even before the spike enters the axon.

Resumption of the AP elicitation when stimuli were decreased below the upper threshold indicates that the upper threshold of stimulation was not associated with cellular damage. It also cannot be explained by the reversible electroporation (formation of pores in cell membrane), since such pores close within tens of seconds to tens of minutes (Bobanović et al. 1999; Saulis 1997), whereas spike generation in our measurements resumed immediately after reduction of the stimulus below the upper threshold, within one period of the stimulation waveform (1 s). Electroporation is also likely to change the cell resting potential, which has not been observed at the upper threshold.

Well-defined upper thresholds could be observed in our measurements only for pulses ≤0.5 ms in duration. For longer pulses, a strong interference between the AP and the stimulus artifact made the determination of the presence of the elicited AP very difficult. For this reason the upper threshold has not been plotted for durations exceeding 0.5 ms in Fig. 4. A similar effect was evident in the modeling (Boinagrov et al. 2010), as well. The upper threshold was not plotted for durations exceeding 0.5 ms in Fig. 5*A*, where interference between the ion channel response and the artifact made it impossible to discern the presence of a well-defined AP.

Width of the stimulation window. The lower and upper thresholds, as well as the stimulation window, significantly varied from cell to cell even for the same pulse width. For example, with 0.2-ms pulses, the stimulation window varied from 2.0 to 7.6, and with 0.5-ms pulses, from 1.8 to 6.4. Such variations in the stimulation thresholds and the stimulation window could be due to the differences in size, shape, and position of the target cell, as well as in uniformity of electric field.

Electrochemical limits of the stimulating electrode depend on its material. One of the popular electrode materials, sputtered iridium oxide (SIROF), can deliver up to 5 mC/cm^2 via an electrode of 30 μm in diameter, with the use of 0.5-ms pulses (Cogan et al. 2004). These settings correspond to the maximum current of 70 μA, which is 16–175 times higher than the stimulation lower threshold at this pulse duration, and can significantly exceed the stimulation upper threshold.

In the histological studies of the cortical tissue damage by prolonged electrical stimulation (McCreery et al. 1990), no damage was observed during stimulation with the charge of 100 nC per phase, even when the charge density was 1 mC/cm^2. For 0.5-ms pulses and an electrode located 25 μm away from the stimulated cell, these values correspond to the current exceeding 150 μA, significantly higher than the upper stimulation threshold. The cellular damage due to electroporation occurs at amplitudes more than 30 times above the lower stimulation threshold (Butterwick et al. 2007). Therefore, the limiting factor in extracellular stimulation of RGCs is likely the upper threshold rather than the electrode or cellular damage.

Strong stimuli applied via epiretinal electrode may preclude spiking of RGCs located right under it, but it may elicit response from a number of more remote RGCs where stimulation will fall into the range between the upper and lower stimulation thresholds. Therefore, predicting perceptual effects of such a complex interplay is quite difficult.

Conclusions. We experimentally confirmed the existence of the upper threshold of extracellular stimulation in retinal ganglion cells at pulse durations ranging from 5 to 500 μs. The ratio of the upper to lower stimulation thresholds with cathodic pulses typically varied from 1.7 to 7.6. Computational modeling of RGC stimulation indicated that the upper threshold is due to reversal of the sodium current at high levels of depolarization, which was further confirmed in experiments with the low-sodium medium. Since the stimulation window can be quite narrow, care should be taken to verify the adequate range of stimulation for any particular neuron in practical applications.

GRANTS

This project was supported in part by National Eye Institute Grant R01 EY018608, a Stanford University Bio-X Research Grant, Air Force Office of Scientific Research Grant FA9550-10-1-0503, and an SU2P Research Council UK Science Bridges award.

DISCLOSURES

No conflicts of interest, financial or otherwise, are declared by the authors.

AUTHOR CONTRIBUTIONS

D.B., S.P.-F., K.M., and D.P. conception and design of research; D.B., B.S., and N.N. performed experiments; D.B. analyzed data; D.B., S.P.-F., K.M., and D.P. interpreted results of experiments; D.B. prepared figures; D.B. drafted manuscript; D.B., K.M., and D.P. edited and revised manuscript; D.B., S.P.-F., B.S., K.M., N.N., and D.P. approved final version of manuscript.

REFERENCES

Bobanović F, Bootman MD, Berridge MJ, Parkinson NA, Lipp P. Elementary $[Ca^{2+}]_i$ signals generated by electroporation functionally mimic those evoked by hormonal stimulation. *FASEB J* 13: 365–376, 1999.

Boinagrov D, Loudin J, Palanker D. Strength-duration relationship for extracellular neural stimulation: numerical and analytical models. *J Neurophysiol* 104: 2236–2248, 2010.

Breit S, Schulz JB, Benabid AL. Deep brain stimulation. *Cell Tissue Res* 318: 275–288, 2004.

Brummer SB, Turner MJ. Electrical stimulation with Pt electrodes: II-estimation of maximum surface redox (theoretical non-gassing) limits. *IEEE Trans Biomed Eng* 24: 440–443, 1977.

Buitenweg JR, Rutten WLC, Marani E. Extracellular stimulation window explained by a geometry-based model of the neuron-electrode contact. *IEEE Trans Biomed Eng* 49: 1591–1599, 2002.

Butterwick A, Vankov A, Huie P, Freyvert Y, Palanker D. Tissue damage by pulsed electrical stimulation. *IEEE Trans Biomed Eng* 54: 2261–2267, 2007.

Cogan SF, Ehrlich J, Plante TD, Smirnov A, Shire DB, Gingerich M, Rizzo JF. Sputtered iridium oxide films (SIROFs) for neural stimulation electrodes. *Conf Proc IEEE Eng Med Biol Soc* 6: 4153–4156, 2004.

Fohlmeister JE, Miller RF. Impulse encoding mechanisms of ganglion cells in the tiger salamander retina. *J Neurophysiol* 78: 1935–1947, 1997.

Fried SI, Hsueh HA, Werblin FS. A method for generating precise temporal patterns of retinal spiking using prosthetic stimulation. *J Neurophysiol* 95: 970–978, 2006.

Fried SI, Lasker ACW, Desai NJ, Eddington DK, Rizzo JF 3rd. Axonal sodium-channel bands shape the response to electric stimulation in retinal ganglion cells. *J Neurophysiol* 101: 1972–1987, 2009.

Greenberg RJ, Velte TJ, Humayun MS, Scarlatis GN, de Juan E Jr. A computational model of electrical stimulation of the retinal ganglion cell. *IEEE Trans Biomed Eng* 46: 505–514, 1999.

Godec C, Cass AS, Ayala GF. Bladder inhibition with functional electrical stimulation. *Urology* 6: 663–666, 1975.

Hodgkin AL, Huxley AF. A quantitative description of membrane current and its application to conduction and excitation in nerve. *J Physiol* 117: 500–554, 1952.

House WF, Urban J. Long term results of electrode implantation and electronic stimulation of the cochlea in man. *Ann Otol Rhinol Laryngol* 82: 504–17, 1973.

Jankowska E, Roberts WJ. An electrophysiological demonstration of the axonal projections of single spinal interneurones in the cat. *J Physiol* 222: 597–622, 1972.

Jensen RJ, Rizzo JF 3rd, Ziv OR, Grumet A, Wyatt J. Thresholds for activation of rabbit retinal ganglion cells with an ultrafine, extracellular microelectrode. *Invest Ophthalmol Vis Sci* 44: 3533–3543, 2003.

Jensen RJ, Ziv O, Rizzo JF 3rd. Thresholds for activation of rabbit retinal ganglion cells with relatively large, extracellular microelectrodes. *Invest Ophthalmol Vis Sci* 46: 1486–1496, 2005.

Jensen RJ, Rizzo JF 3rd. Thresholds for activation of rabbit retinal ganglion cells with a subretinal electrode. *Exp Eye Res* 83: 367–373, 2006.

Katz B, Miledi R. Propagation of electric activity in motor nerve terminals. *Proc R Soc Lond B Biol Sci* 161: 453–482, 1965.

Kern DS, Kumar R. Deep brain stimulation. *Neurologist* 13: 237–252, 2005.

Kimberley TJ, Lewis SM, Auerbach EJ, Dorsey LL, Lojovich JM, Carey JR. Electrical stimulation driving functional improvements and cortical changes in subjects with stroke. *Exp Brain Res* 154: 450–460, 2004.

Krauss JK, Yianni J, Loher TJ, Aziz TZ. Deep brain stimulation for dystonia. *J Clin Neurophysiol* 21: 18–30, 2004.

Kumar K, Toth C, Nath RK. Deep brain stimulation for intractable pain: a 15-year experience. *Neurosurgery* 40: 736–747, 1997.

Kringelbach ML, Jenkinson N, Owen SL, Aziz TZ. Translational principles of deep brain stimulation. *Nat Rev Neurosci* 8: 623–635, 2007.

Leone M. Deep brain stimulation in headache. *Lancet Neurol* 5: 873–877, 2006.

Long DM, Erickson D, Campbell J, North R. Electrical stimulation of the spinal cord and peripheral nerves for pain control. *Appl Neurophysiol* 44: 207–217, 1981.

Mayberg HS, Lozano AM, Voon V, McNeely HE, Seminowicz D, Hamani C, Schwalb JM, Kennedy SH. Deep brain stimulation for treatment-resistant depression. *Neuron* 45: 651–660, 2005.

McCreery DB, Agnew WF, Yuen TGH, Bullara L. Charge density and charge per phase as cofactors in neural injury induced by electrical stimulation. *IEEE Trans Biomed Eng* 37: 996–1001, 1990.

Palanker D, Vankov A, Huie P, Baccus S. Design of a high resolution optoelectronic retinal prosthesis. *J Neural Eng* 2: S105–S120, 2005.

Perlmutter JS, Mink JW. Deep brain stimulation. *Annu Rev Neurosci* 29: 229–257, 2006.

Plaha P, Gill SS. Bilateral deep brain stimulation of the pedunculopontine nucleus for Parkinson's disease. *Neuroreport* 16: 1883–1887, 2005.

Ranck J Jr. Which elements are excited in electrical stimulation of mammalian central nervous system: a review. *Brain Res* 98: 417–440, 1975.

Rizzo JF 3rd, Wyatt J. Prospects for a visual prosthesis. *Neuroscientist* 3: 251–262, 1997.

Sakmann B, Neher E. Patch clamp techniques for studying ionic channels in excitable membranes. *Annu Rev Physiol* 46: 455–72, 1984.

Saulis G. Pore disappearance in a cell after electroporation: theoretical simulation and comparison with experiments. *Biophys J* 73: 1299–1309, 1997.

Sekirnjak C, Hottowy P, Sher A, Dabrowski W, Litke AM, Chichilnisky EJ. Electrical stimulation of mammalian retinal ganglion cells with multi-electrode arrays. *J Neurophysiol* 95: 3311–3327, 2006.

Sekirnjak C, Hottowy P, Sher A, Dabrowski W, Litke AM, Chichilnisky EJ. High-resolution electrical stimulation of primate retina for epiretinal implant design. *J Neurosci* 28: 4446–4456, 2008.

Spelman FA. The past, present, and future of cochlear prostheses. *IEEE Eng Med Biol Mag* 18: 27–33, 1999.

Stett A, Barth W, Weiss S, Haemmerle H, Zrenner E. Electrical multisite stimulation of the isolated chicken retina. *Vision Res* 40: 1785–1795, 2000.

Stett A, Mai A, Herrmann T. Retinal charge sensitivity and spatial discrimination obtainable by subretinal implants: key lessons learned from isolated chicken retina. *J Neural Eng* 4: S7–S16, 2007.

Tsai D, Morley JW, Gregg J, Suaning GJ, Lovell NH. Direct activation and temporal response properties of rabbit retinal ganglion cells following subretinal stimulation. *J Neurophysiol* 102: 2982–2993, 2009.

Vercueil L, Pollak P, Fraix V, Caputo E, Moro E, Benazzouz A, Xie J, Koudsie A, Benabid AL. Deep brain stimulation in the treatment of severe dystonia. *J Neurol* 248: 695–700, 2001.

Weiland JD, Liu W, Humayun MS. Retinal prosthesis. *Annu Rev Biomed Eng* 7: 361–401, 2005.

Zierhofer C, Hochmair-Desoyer I, Hochmair E. Electronic design of a cochlear implant for multichannel high-rate pulsatile stimulation strategies. *IEEE Trans Rehabil Eng* 3: 112–116, 1995.

Zrenner E, Bartz-Schmidt KU, Benav H, Besch D, Bruckmann A, Gabel VP, Gekeler F, Greppmaier U, Harscher A, Kibbel S, Koch J, Kusnyerik A, Peters T, Stingl K, Sachs H, Stett A, Szurman P, Wilhelm B, Wilke R. Subretinal electronic chips allow blind patients to read letters and combine them to words. *Proc R Soc Lond B Biol Sci* 278: 1489–1497, 2011.